Applied Mechanics and Materials
ISSN: 1662-7482, Vol. 575, pp 315-321
doi:10.4028/www.scientific.net/AMM.575.315

Submitted: 2014-04-24
Accepted: 2014-04-25
Online: 2014-06-25

Effect of annealing temperature on microstructures and properties of warmly deformed SCRAM steel

Yang Mou[a], Lihong Xue[a],*, Qilai Zhou[a], Caixuan Lu[a], Jinping Suo[a], Liping Guo[b],Youwei Yan[a]

[a]State Key Laboratory of Mould Technology, Institute of Materials Science and Engineering, Huazhong University of Science and Technology, Wuhan 430074, PR China
[b]Key Laboratory of Artificial Micro- and Nano-structures of Ministry of Education and School of Physics and Technology, Wuhan University, Wuhan 430072, China

*Corresponding author: Tel.: +86 2787558290
Fax: +86 2787541922
E-mail address: xuelh@mail.hust.edu.cn (L. Xue)

Keywords: annealing temperature, warm deformation, martensitic lath width, dislocation density, helium bubbles, nano-indentation hardness

Abstract

Effect of annealing temperature on microstructures and properties of warmly deformed SCRAM (Super-clean Reduced Activation Martensitic) steel on Gleeble-3500 thermo-simulation machine was investigated. The results showed that an increase in the annealing temperature can result in increasing the martensitic lath width from 0.48 um to 0.65 um and decreasing the dislocation density from 6.4×10^{15} m^{-2} to 2.8×10^{15} m^{-2} in SCRAM steel. The specimen exhibited high reduction of area and total elongations when the annealing temperature is up to 600 ºC. The tensile fracture surface observation indicated that dimples became more uniform and deeper and cleavage fracture traces disappeared with the annealing temperature increasing. The irradiation-induced helium bubbles and hardening were observed in all the specimens after helium implantation to 1e + 17/cm^2 at 450 ºC. The helium bubbles became larger but less when the annealing temperature increased. The optimal annealing temperature is 450 ºC in this experiment.

Introduction

Reduced-activation ferritic/martensitic (RAFM) steels are presently considered as one of the most realistic candidates for the structural materials of fusion blanket systems [1, 2]. Several typical RAFM steels are selected as primary blanket structural materials in the prospective International Thermonuclear Experimental Reactor (ITER) including F82H, JLF-1, EUROFER97, 9Cr2WVTa and CLAM steel [3~5].The SCRAM steel is a new RAFM steel [6], which was developed by our group using Cr-W-V-Ti-N system instead of Cr-W-V-Ta system. The SCRAM steel exhibited better low activation and good mechanical properties compared to other RAFM steels.

Helium is one of the major nuclear transmutation products in structural materials of fusion reactors [7]. It can stabilize a point defect cluster and cause additional hardening in the lower temperature region and an increase in swelling in the higher temperature region. This will cause detrimental effect on the mechanical properties of RAFM steels. In previous studies, Kimura et al. [8] have found that the decrease in grain size and the increase in dislocation density can increase the

trapping capacity of helium in the martensitic structure and reduce detrimental effects of helium bubble on mechanical properties.

Warm deformation was introduced to decrease grain size and increase dislocation density in previous research to improve the resistance to irradiation of SCRAM steel. However, the specimens exhibited low reduction of area and low total elongations simultaneously. Good comprehensive properties of the SCRAM steel are required in ITER application. It is well known that appropriate annealing treatment can eliminate the internal residual stress of materials, restrain grains from growing up, adjust microstructure structure and composition and then enhance the plasticity and toughness of materials [9]. In order to improve the comprehensive properties of warmly deformed SCRAM steel, the effect of annealing temperature on microstructures and properties of warmly deformed SCRAM steel was investigated in this paper.

Experimental procedure

Table 1: Chemical compositions of the SCRAM steel.

Element	C	Si	Mn	Cr	W	V	Ti	P	S	O	N	Fe
wt.%	0.088	0.28	0.5	9.3	2.28	0.094	0.011	0.0056	0.002	0.0038	0.0150	Bal.

The chemical compositions of the SCRAM steel used in this study are listed on Table 1. The steel was melted by vacuum induction melting and electro-slag remelting at argon atmosphere into an ingot of 100 kg, followed by hot-forging and rolling into ø24 mm rods. Subsequently, this steel was heat-treated by twice quenching and tempering processes: 980 ºC/0.5 h/W.C (water cool) + 760 ºC/2 h/A.C (air cool); 960 ºC/0.5 h/W.C (water cool) + 740 ºC/2 h/A.C (air cool). More detailed information on the preparation of SCRAM steel can be obtained in our published reference [6].

Cylindrical specimens with size of ø8mm×12mm were cut along the rolling direction by wire electrode discharging. The warm deformation was performed on Gleeble-3500 thermo-simulation machine. Before deformation, the specimens were heated to 600 ºC at a heating rate of 5 ºC/s, and isothermally held for 5 min. Then the specimens were deformed at strain ε=0.5 at strain rate of 0.01 s^{-1} followed by air cooling immediately. Subsequently, the annealing treatment was conducted on the deformed specimens at different temperature (0-600 ºC) for 2h in chamber electric furnace.

The annealing specimens were cut into 0.5 mm thickness slices in the center parallel to the compressive direction by wire electrode discharging, and ground into ~30 μm in thickness using different grit papers. Standard transmission electron microscopy (TEM) disc specimens of 3 mm in diameter were punched and then thinned into perforation on a twin jet electro-polisher with 10% $HClO_4$ in glacial acetic acid at temperature of 10 ºC and potential of 40 V.

Helium implantation was carried out by an implantation apparatus located in the Accelerator Lab of Wuhan University. The SCRAM steels were implanted by using 18 keV helium beam with fluencies up to 1e + 17/cm^2 at 450 ± 10 ºC.

Microstructures of annealing specimens before and after helium implantation were examined from the direction parallel to the compressive direction by using an optical microscope and a JEM-2010 transmission electron microscope (TEM) operated at 200 kV. The thickness of the TEM observation areas was deduced from the number of thickness fringes.

Tensile tests were measured on Instron 5848 micro-tester at a strain rate of 2×10^{-3} s^{-1} at room temperature. Dog-bone tensile specimens with gauge size of 5mm×2mm×1mm were prepared by cutting out in the center of warmly deformed specimens in the transverse direction by wire electrode discharging and hand lapping by diamond abrasive paste. The fracture morphology of

tensile specimen was observed on a Nova NanoSEM 450 scanning electron microscope (SEM) at 2 kV.

Results and discussion

The typical bright-field TEM micrographs of the warmly deformed specimens after different annealing temperature for 2 h are shown in Fig. 1 The width of martensitic laths slightly increased and many subgrains were generated inside martensitic laths with the annealing temperature increasing. The elongated and equiaxed carbides or carbonitrides precipitated out mainly along lath boundaries and subgrain boundaries. The martensitic lath width can be determined by counting the number of intersections of lath boundaries with straight lines vertical to elongated direction of lath grains. To ensure reliable lath width and the mean diameter and the volume fraction of precipitates measurements, at least 5 different micrographs were investigated for each sample. The calculated results are presented in Table 2. The average lath width was measured as 0.48 μm, 0.53 μm, 0.65 μm for the annealing temperature of 0 ºC, 450 ºC, 600 ºC, respectively. The mean diameter of precipitates decreased from 99 nm (0 ºC) to 82 nm (600 ºC) for these specimens while the volume fraction of precipitates drastically increased from 5.56% (0 ºC) to 5.92% (600 ºC).

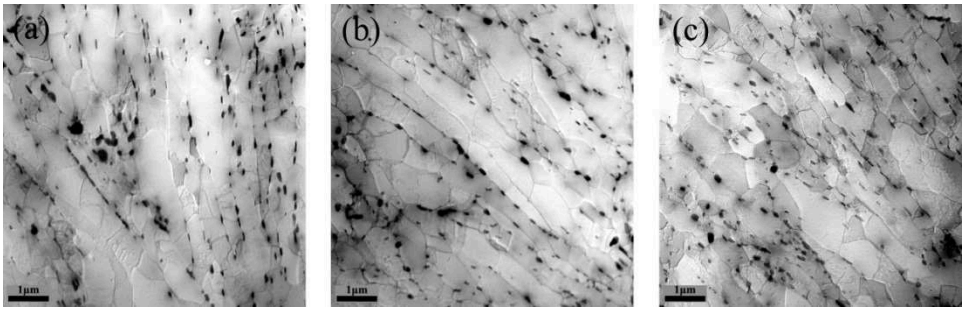

Fig. 1 TEM micrographs of thin foil samples after different annealing temperature at (a) 0 ºC, (b) 450 ºC, (c) 600 ºC for 2h for martensitic lath.

Fig.2 shows high magnification TEM micrographs of thin foil samples after different annealing temperature for the SCRAM steel. Fig.2 (a) shows dislocation cells and heavy dislocation tangle were formed before annealing treatment. When the annealing temperature was up to 450 ºC in Fig.2 (b), free dislocation progressively decreased and gathered to grain boundaries. Dislocation density greatly decreased and a great number of dislocation cells were formed with the annealing temperature further increasing to 600 ºC.

The dislocation density was calculated by the following equation [11]:

$$\rho = \frac{1}{t}\left(\frac{\sum n_v}{\sum L_v} + \frac{\sum n_h}{\sum L_h}\right) \quad (1)$$

Where t is the foil thickness varied between 180 and 220 nm. The measurement of dislocation density was performed using two sets of horizontal (L_h) and vertical (L_v) reference lines which was superimposed in the center of the sub-grains. The numbers n_v and n_h of intersections of dislocations with the vertical (L_v) and horizontal (L_h) grid lines were counted [12].

At least 5 images from different fields of view were investigated and the quantitative determination of dislocation density was obtained for each sample. The dislocation density was measured as 6.4×10^{15} m^{-2}, 5.1×10^{15} m^{-2}, 2.8×10^{15} m^{-2} for the annealing temperature of 0 ºC, 450 ºC, 600 ºC shown in Table 2, respectively. The order of 10^{15} m^{-2} is consistent to the dislocation density level of martensitic steels [13, 14].

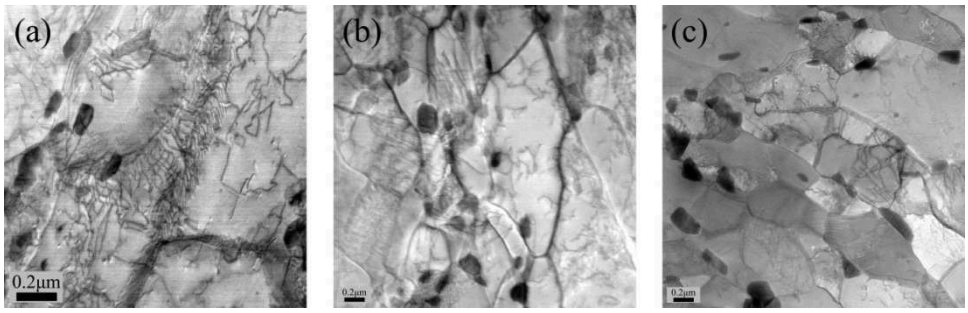

Fig. 2. High magnification TEM micrographs of thin foil samples after different annealing temperature at (a) 0 ºC, (b) 450 ºC, (c) 600 ºC for 2h for dislocation density.

Table 2: Quantitative determination of mean diameter of lath width, dislocation density, the mean diameter and the area fraction of precipitates for SCRAM steels after three annealing temperature.

Annealing temperature(ºC)	Mean diameter of laths (μm)	Dislocation density (m^{-2})	Mean diameter of precipitates (nm)	Area fraction of precipitates (%)
0	0.48	6.4×10^{15}	99	5.56%
450	0.53	5.1×10^{15}	93	5.70%
600	0.65	2.8×10^{15}	82	5.92%

Variation of tensile properties of these specimens is presented in Table 3. The SEM micrographs of the tensile fracture surfaces of the specimens are shown in Fig. 3. The sample before annealing treatment exhibited the highest ultimate tensile strength (748 MPa) and yield strength (632 MPa) but the lowest reduction of area (52.6%) and total elongations (12.5%), respectively. A typical brittle fracture and huge radial tear ridges were clearly observed in the tensile fracture surfaces (Fig. 3(a) and (d)). The results suggested that strain hardening had been introduced in SCRAM steels during warm deformation. An increase in annealing temperature resulted in an increase in the reduction of area and total elongations. It can be seen that dimples became larger and deeper from the tensile fracture surfaces. Saeidiet al. [15] reported that large and deep dimples indicate more toughness in steels. When the annealing temperature reached 600 ºC, the sample exhibited highest the reduction of area (71.8%) and total elongations (21.5%), respectively. No obvious brittle fracture trace was observed from Fig. 3(c) and (f), which meaned that strain hardening had been effectively mitigated.

Table 3: Tensile properties of SCRAM steel after different annealing temperature.

Annealing temperature (ºC)	Ultimate tensile strength (MPa)	Yield strength (MPa)	Total elongations (%)	Reduction of area (%)
0	748	632	12.5	52.6
450	725	596	18.4	64.9
600	691	547	21.5	71.8

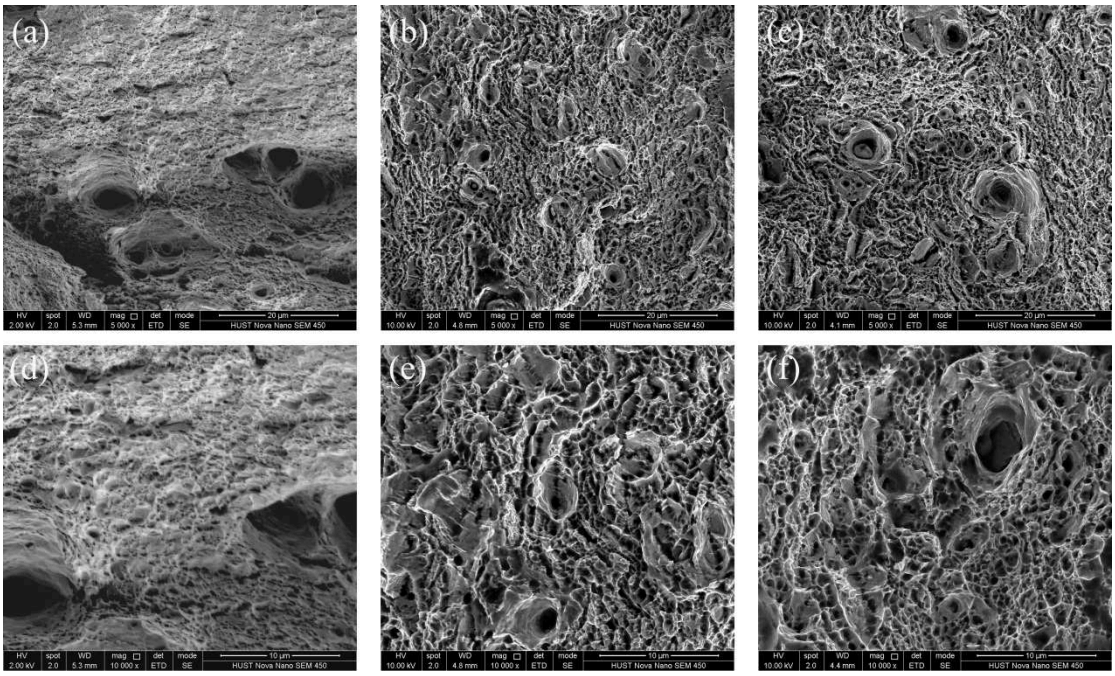

Fig. 3. SEM micrographs of the tensile fracture surface after different annealing temperature at (a) (d) 0 ºC, (b) (e) 450 ºC, (c) (f) 600 ºC for 2h for dislocation density.

TEM micrographs at high magnification of the annealing SCRAM steel after helium implantation to 1e + 17/cm2 at 450 ºC are shown in Fig. 4. The irradiation-induced helium bubbles can be observed in all the specimens. The bubbles were preferentially nucleated and aggregated at prior austenitic grain boundaries, lath boundaries and sub-boundaries as well as dislocations inside the laths and carbide-matrix interfaces, consistent to the results of previous studies [16, 17].

Fine bubbles were observed in the steel before annealing treatment (Fig. 4(a) and (c)). They were found to be distributed uniformly and no obvious bubble segregation on boundaries was observed. The average diameter of bubbles was 2.3 nm and the number density reached 3.2×10^{23} m^{-3}. In the annealing steel at 450 ºC, the average size of bubbles was larger and the bubble distribution became more inhomogeneous (Fig. 4(b) and (e)), with a number density of 2.9×10^{23} m^{-3} and the average diameter of 2.8 nm. It can be seen that the distribution of bubbles was inhomogeneous in the annealing steel at 600 ºC (Fig. 4(c) and (f)). A great number of large bubbles were observed mainly nucleated at dislocations inside the laths and boundaries. The mean diameter of bubbles was 3.9 nm and the number density was 2.3×10^{23} m^{-3}.

The size distribution of helium bubbles in SCRAM specimens calculated based on TEM micrographs (Fig. 4) are presented in Fig. 5. It clearly showed the bubble size tended to increase with the annealing temperature increasing.

The variation trend of helium bubbles could be contributed by a large number of trapping sites, namely dislocations and lath boundaries, disappeared in the SCRAM steels after annealing treatment. Because of few dislocations and lath boundaries in matrix, most of helium atoms produced by irradiation were aggregated and nucleated at such trapping sites. Consequently, helium bubbles grow to large size in annealing sample during helium implantation.

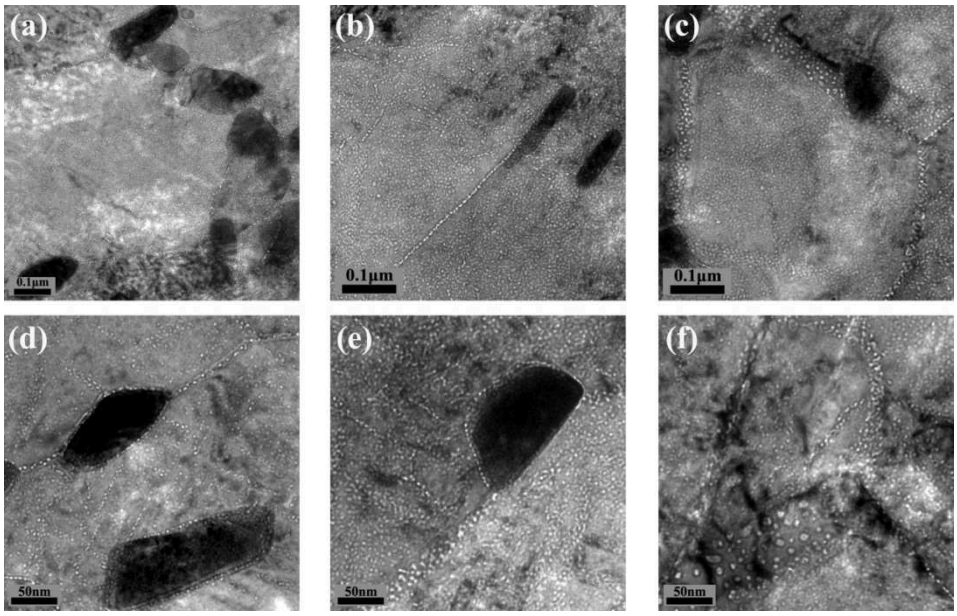

Fig. 4. TEM micrographs showing helium bubbles structure in annealing SCRAM steel after helium implantation to 1e + 17/cm2 at 450 ºC: (a) (d) 0 ºC, (b) (e) 450 ºC, (c) (f) 600 ºC for 2h

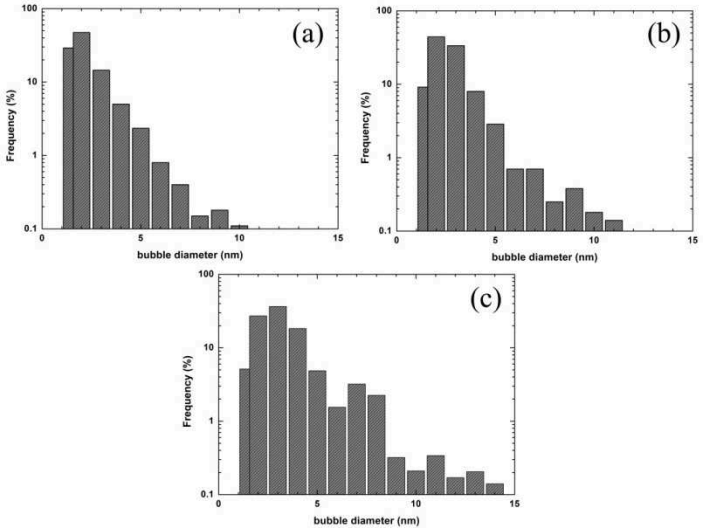

Fig. 5. Size distribution of helium bubbles in annealing SCRAM steel after helium implantation to 1e + 17/cm2 at 450 ºC: (a) 0 ºC, (b) 450 ºC, (c) 600 ºC for 2h.

Although annealing treatment of the SCRAM steel can increase the reduction of area and total elongations, it can cause the decrease in the dislocation density and the increase in martensitic lath width before irradiation. This weakened helium trapping capacity of martensitic matrix resulting in helium bubbles growth up and ΔH increasing. Considering the comprehensive properties of SCRAM steel before and after irradiation, 450 ºC is the optimal annealing temperature in this experiment.

Summary

The effect of annealing temperature on microstructures and properties of warmly deformed SCRAM steel has been investigated. The main conclusions can be summarized as following:

(1) As annealing temperature increasing, the martensitic lath width increased from 0.48 um to 0.65 um and the dislocation density decreased from 6.4×10^{15} m^{-2} to 2.8×10^{15} m^{-2} in SCRAM steel. The specimen exhibited high reduction of area and total elongations when the annealing temperature was up to 600 ºC. The tensile fracture surface observation indicated that dimples

became more uniform and deeper and cleavage fracture traces disappeared with the annealing temperature increasing.

(2) The irradiation-induced helium bubbles and hardening were observed in all the specimens after helium implantation to 1e + 17/cm^2 at 450 ºC. The helium bubbles became larger but less when the annealing temperature increased.

(3) Considering the comprehensive properties of SCRAM steel before and after irradiation, 450 ºC is the optimal annealing temperature in this experiment.

Reference

[1] Yu JN, Huang QY, Wan FR. Research and development on the China low activation martensitic steel (CLAM). J Nucl Mater 2007; 367: 97-101.
[2] H. Tanigawa, K. Shiba, H. Sakasegawa, et al., Fus. Eng. Des. 86 (2011) 2549–2552
[3] A. Kimura, R. Kasada, A. Kohyama, et al., J. Nucl. Mater. 367–370 (2007) 60–67.
[4] N. Baluc, D.S. Gelles, S. Jitsukawa, et al., J. Nucl. Mater. 367–370 (2007) 33–41.
[5] Q. Huang, C. Li, et al., J. Nucl. Mater. 367–370 (2007) 142–146.
[6] X. S. Xiong, F. Yang, X. R. Zou, et al., J. Nucl. Mater. 430 (2012) 114-118.
[7] R.L. Klueh, D.S. Gelles, S. Jitsukawa et al., J. Nucl. Mater. 307-311 (2002) 455.
[8] A. Kimura, R. Kasada, K. Morishita, et al., J. Nucl. Mater. 307-311 (2002) 521-526.
[9] Z. Q. Cui, Y. C. Xun, Metallography and Heat Treatment, secnnd ed., Metallurgical Industry Press, Beijing, 2007.
[10] W.C. Oliver, G.M. Pharr, J. Mater. Res. 7 (1992) 1564.
[11] J. Pěsička, R. Kužul, A. Dronhofer, G. Eggeler, Acta Mater. 51 (2003) 4847-4862.
[12] D. Rojas, J. Garcia, O. Prat et al., Mater. Sci. Eng. A528 (2011) 1372-1381.
[13] K. Takasawa, R. Ikeda et al., Int J Hydrogen Energy 37 (2012) 2669-2675.
[14] B. Hoffmann, O. Vöhringer , E. Macherauch, Mater. Sci. Eng. A319–321 (2001) 299-303.
[15] N. Saeidi, A. Ekrami, Mater. Sci. Eng. A527 (2010) 5575-5581.
[16] J. Henry, M.-H. Mathon, P. Jung, J. Nucl. Mater. 318 (2003) 249-259.
[17] S. Fréchard, M. Walls, M. Kociak, et al., J. Nucl. Mater. 393 (2009) 102-107.